Sound radiation from a submerged stiffened cylinder with acoustic excitation

James A. Forrest

Maritime Division, Defence Science and Technology Group, Melbourne, Australia

ABSTRACT

The sound radiated from an underwater cylindrical enclosure with an internal noise source can be modelled analytically by combining a number of mathematical results. The scattered sound field due to a monopole source in the cylindrical volume provides the internal pressure loading on the cylinder walls; the response of the cylinder is calculated using this loading as the forcing term in a thin-shell theory formulation including external fluid loading; and the far-field radiated sound is then calculated using the cylindrical shell response as the input to an expression for this. Previous work applied this approach with an isotropic cylindrical shell and considered the effect of multiple noise sources and the incorporation of internal acoustic damping. This paper considers the extension of this model to allow for a cylindrical shell with longitudinal and/or circumferential stiffeners. Radiated sound calculated using the isotropic shell and variations on the stiffened shell is compared.

1. INTRODUCTION

Sound radiated from submerged or water-loaded structures is of interest for a number of areas in the maritime domain. These include far-field radiated noise or self-noise impact on sonar performance for naval vessels, self-noise impact on sonar imaging systems for hydrographic vessels, and the environmental impact of underwater radiated noise. Analytical methods based on mathematical modelling can give useful insights into several classes of underwater structural acoustics problems, usually with shorter computation times than numerical alternatives such as fully coupled finite-element (FE) / boundary element (BE) methods. The numerical methods come into their own, however, for more complicated built-up structures for which analytical solution is intractable. Junger & Feit (1993) and Skelton & James (1997) describe a range of analytical methods applicable to underwater structural acoustics.

This paper considers the extension of an analytical model originally developed by James (1985) for a submerged cylindrical enclosure with an internal noise source. This model calculates the sound radiated from the cylinder by combining a number of mathematical results. The scattered sound field due to a monopole source in the cylindrical volume provides the internal pressure loading on the cylinder walls; the response of the cylinder is calculated using this loading as the forcing term in a thin-shell theory formulation including external fluid loading; and the far-field radiated sound is then calculated using the cylindrical shell response as the input to an expression for this. The model has been validated by comparison to FE/BE results by Pan, MacGillivray, Tso & Peters (2013). The model has also been extended by Pan, Tso, Forrest & Peters (2014) to consider multiple monopole sources with independent magnitudes and phases in order to model distributed internal noise sources; and to include the effect of acoustic damping material based on the Sabine absorption coefficient, with further validation against FE/BE models. The Sabine theory is described in texts such as Bies & Hansen (1996).

However, cylindrical structures usually incorporate stiffening elements such as circumferential ribs or longitudinal stringers, which are not accounted for in the James (1985) model or the extensions described above. Stiffening elements affect basic wave propagation behaviour in a cylindrical shell, as shown in Forrest (2011), as well as its overall forced vibration response, as shown in Forrest (2014). For the low frequency range, i.e. where the structural wavelengths are larger than the spacing of the stiffening elements, a good approximation is to include the extra mass and stiffness of ribs or stringers as smeared properties in the shell. The equations of motion for the original isotropic shell are replaced with those for an orthotropic shell which include the smeared stiffener properties. A modified version of the formulation of Mikulas & McElman (1965), summarised in Leissa (1993), is used in this paper to represent stiffeners added to the cylindrical enclosure.

The following sections describe the modifications to the shell equations of motion, their incorporation with the other parts of the model that determine the internal acoustic excitation and the far-field radiated sound, and some results from the model including T-section stiffeners. Two separate cases are considered in the results section to demonstrate the model: one with circumferential ribs, and one with longitudinal stringers. In each case, results

are compared for the plain shell, the shell with added stiffener mass only, and the orthotropic shell with full representation of smeared rib or stringer mass and stiffness.

2. MATHEMATICAL MODEL

2.1 Geometry of the submerged cylindrical shell

The geometry and coordinate systems for the submerged cylindrical shell are shown in Figure 1. The shell has a length of $2L$, radius of a and thickness of h. It has semi-infinite rigid baffles attached at each end, indicated as the fine dotted lines. It encloses a finite cylindrical acoustic volume. Sound radiation from the endplates into the exterior fluid is not considered. The cylinder therefore can be seen as representing a section of a larger structure. The global origin is at the centre of the cylindrical enclosure formed by the shell. The shell motion is described in terms of a shell-surface cylindrical coordinate system with axial displacement u, tangential displacement v and radial displacement w. The internal pressure p_i is defined in terms of a cylindrical coordinate system (r, ϕ, z). The displacement components (u, v, w) have been given directions to match the right-handed system defined by the cylindrical coordinates (r, ϕ, z). While this reverses the direction of v conventionally used in thin-shell theory, where (u, v, w) define the right-handed system, the direction of the circumferential angle ϕ is also reversed. The net result is that all terms in the equations of motion for a thin shell retain their relative signs. In any case, the internal and external fluid pressures only couple to the cylindrical shell through the radial component w. Lastly, the far-field radiated pressure p_{ef} is defined in terms of a spherical coordinate system (R, θ, ϕ), where θ is the angle from the z-axis. Various physical assumptions used to solve the problem will be described at the appropriate points.

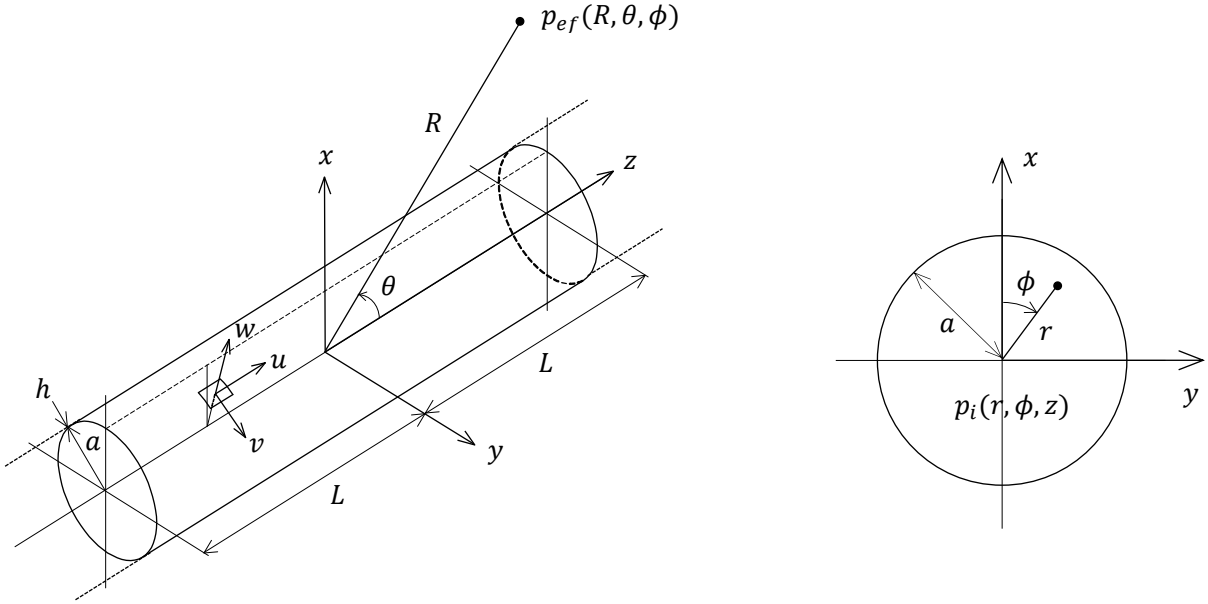

Figure 1: Isometric projection and cross-section of the cylindrical shell with the various coordinate systems used

2.2 Response of the cylindrical shell with stiffeners

Firstly, the motion of the cylindrical shell including stiffeners needs to be described. The shell equations of motion used by James (1985) are based on the Arnold-Warburton version of thin-shell theory. There are a number of different thin-shell theories, which are surveyed in Leissa (1993). The simplest equations including shell bending are those of Donnell-Mushtari, which are the basis of the stiffened shell results given by Mikulas & McElman (1965). The more complicated versions, such as those of Arnold-Warburton and Flügge, include extra terms for the bending of the shell, and can give more accurate results for thicker shells and/or to higher frequencies. Mikulas & McElman (1965) consider bending, extension and twisting of the stiffeners imparted by the motion of the cylindrical shell to which they are fixed, but ignore in-plane inertia, including the effect of shell and stiffener mass only in the radial direction. The equations of motion based on Arnold-Warburton theory with added longitudinal stiffeners and

circumferential ribs, including inertia and arbitrary loading in all three directions, are given below. They represent equilibrium in each of the axial, tangential and radial directions respectively.

$$-\left(E_1+k_{A_s}\right)u_{zz}-\frac{E_1(1-\nu)}{2a^2}u_{\phi\phi}+\rho_t h\ddot{u}-\frac{E_1(1+\nu)}{2a}v_{z\phi}-\frac{E_1\nu}{a}w_z+\bar{z}_s k_{A_s}w_{zzz}=f_1 \tag{1}$$

$$-\frac{E_1(1+\nu)}{2a}u_{z\phi}-E_1(1-\nu)\left(\frac{1}{2}+2\beta^2\right)v_{zz}-\frac{1}{a^2}\left(E_1(1+\beta^2)+k_{A_r}\right)v_{\phi\phi}+\rho_t h\ddot{v}-\frac{1}{a^2}\left(E_1+k_{A_r}\right)w_\phi+$$
$$E_1\beta^2(2-\nu)w_{zz\phi}+\frac{1}{a^2}\left(E_1\beta^2+\frac{\bar{z}_r k_{A_r}}{a}\right)w_{\phi\phi\phi}=f_2 \tag{2}$$

$$\frac{E_1\nu}{a}u_z-\bar{z}_s k_{A_s}u_{zzz}+\frac{1}{a^2}\left(E_1+k_{A_r}\right)v_\phi-E_1\beta^2(2-\nu)v_{zz\phi}-\frac{1}{a^2}\left(E_1\beta^2+\frac{\bar{z}_r k_{A_r}}{R}\right)v_{\phi\phi\phi}+\frac{1}{a^2}\left(E_1+k_{A_r}\right)w+$$
$$\left(E_1\beta^2a^2+k_{I_s}+\bar{z}_s^2k_{A_s}\right)w_{zzzz}+\left(2E_1\beta^2+\frac{k_{J_r}+k_{J_s}}{a^2}\right)w_{zz\phi\phi}+\frac{1}{a^2}\left(E_1\beta^2+\frac{k_{I_r}+\bar{z}_r^2k_{A_r}}{a^2}\right)w_{\phi\phi\phi\phi}-\frac{2}{a^3}\bar{z}_r k_{A_r}w_{\phi\phi}+$$
$$\rho_t h\ddot{w}=f_3 \tag{3}$$

The subscripts on u, v and w represent differentiation with respect to ϕ or z and dot represents differentiation with respect to time. The terms f_1, f_2 and f_3 are the net external tractions acting in the axial, tangential and radial directions. General shell parameters are defined as

$$\beta^2\equiv\frac{h^2}{12a^2},\quad E_1\equiv\frac{Eh}{1-\nu^2},\quad \rho_t\equiv\rho+\frac{\rho_r A_r}{bh}+\frac{\rho_s A_s}{dh} \tag{4}$$

where E is the Young's modulus and ν is the Poisson's ratio of the shell material. The effective density of the shell is ρ_t, which depends on the density of the shell material ρ; the material density ρ_r, cross-sectional area A_r and longitudinal spacing b of the ribs; and the material density ρ_s, cross-sectional area A_s and circumferential spacing d of the stringers. The distances of the cross-sectional area centroids of the stiffeners to the mid-surface of the shell are $\bar{z}_r$ and $\bar{z}_s$ for the ribs and stringers respectively. These centroidal distances take negative values in the equations of motion (1) to (3) when the stiffeners are inside the shell, and positive values when they are outside. It is convenient to use further rib and stringer parameters defined as

$$k_{A_r}\equiv\frac{E_r A_r}{b},\quad k_{A_s}\equiv\frac{E_s A_s}{d},\quad k_{I_r}\equiv\frac{E_r I_r}{b},\quad k_{I_s}\equiv\frac{E_s I_s}{d},\quad k_{J_r}\equiv\frac{G_r J_r}{b},\quad k_{J_s}\equiv\frac{G_s J_s}{d} \tag{5}$$

where E_r and E_s are the Young's moduli, and G_r and G_s are the shear moduli of the rib and stringer materials; and I_r and I_s are the second moments of area, and J_r and J_s are the torsion constants for the rib and stringer cross-sections. It can be seen that the k_A parameters are related to the axial stiffness of the ribs or stringers, the k_I parameters to the bending stiffness and the k_J parameters to the torsional stiffness.

The cylindrical shell is assumed to be "simply supported" at the ends, otherwise known as shear diaphragm end conditions. This means the radial and tangential displacements are zero at the ends, but the shell is free to move axially and can also rotate about the v-axis around the end circumferences. Solutions for the three displacement components that are time-harmonic with angular frequency ω, and that satisfy these end conditions and the equations of motion, can be written as Fourier series as follows.

$$u=\sum_{m=1}^{\infty}\sum_{n=0}^{\infty}U_{mn}\cos\left(\frac{m\pi(z+L)}{2L}\right)\cos n\phi\,.\,\mathrm{e}^{-\mathrm{i}\omega t} \tag{6}$$

$$v=\sum_{m=1}^{\infty}\sum_{n=0}^{\infty}V_{mn}\sin\left(\frac{m\pi(z+L)}{2L}\right)\sin n\phi\,.\,\mathrm{e}^{-\mathrm{i}\omega t} \tag{7}$$

$$w=\sum_{m=1}^{\infty}\sum_{n=0}^{\infty}W_{mn}\sin\left(\frac{m\pi(z+L)}{2L}\right)\cos n\phi\,.\,\mathrm{e}^{-\mathrm{i}\omega t} \tag{8}$$

This represents the displacements as sums of modes (m,n) characterised by an axial mode number m and a circumferential mode number n. The particular choice of time-harmonic variation means that damping can be

included in the model using complex moduli of the form $E(1-i\eta)$ for Young's modulus, for example, with a damping factor of η.

Substituting the assumed solutions (6) to (8) into the equations of motion (1) to (3) gives a matrix equation for the displacements for each (m,n) pair in the frequency domain of the form

$$\begin{bmatrix} S_{11} & S_{12} & S_{13} \\ S_{21} & S_{22} & S_{23} \\ S_{31} & S_{32} & S_{33} \end{bmatrix} \begin{bmatrix} U_{mn} \\ V_{mn} \\ W_{mn} \end{bmatrix} = \begin{bmatrix} F_{1_{mn}} \\ F_{2_{mn}} \\ F_{3_{mn}} \end{bmatrix} \tag{9}$$

where $F_{1_{mn}}$, $F_{2_{mn}}$ and $F_{3_{mn}}$ are the corresponding spectral components of the axial, tangential and radial tractions. At natural frequencies of the shell with no damping, the determinant of the matrix is zero, and solution of the displacements may be numerically intractable. Inclusion of structural damping alleviates this issue. Including the term for external fluid loading on the shell in the left-hand side of Equation (9) as part of S_{33} and defining the axial wave number as $\alpha_m \equiv \frac{m\pi}{2L}$, the elements of the matrix are given by

$$S_{11} = E_1\left(\alpha_m^2 + \tfrac{(1-\nu)}{2a^2}n^2\right) + k_{A_s}\alpha_m^2 - \rho_t h\omega^2$$

$$S_{12} = -E_1\tfrac{(1+\nu)}{2a}\alpha_m n$$

$$S_{13} = -E_1\tfrac{\nu}{R}\alpha_m - \bar{z}_s k_{A_s}\alpha_m^3$$

$$S_{21} = S_{12}$$

$$S_{22} = E_1\left((1-\nu)\left(\tfrac{1}{2}+2\beta^2\right)\alpha_m^2 + \tfrac{(1+\beta^2)}{a^2}n^2\right) + \tfrac{k_{A_r}}{a^2}n^2 - \rho_t h\omega^2$$

$$S_{23} = E_1\left(\tfrac{n}{a^2} + \beta^2(2-\nu)\alpha_m^2 n + \tfrac{\beta^2}{a^2}n^3\right) + \tfrac{\bar{z}_r k_{A_r}}{a^3}n^3$$

$$S_{31} = S_{13}$$

$$S_{32} = S_{23}$$

$$S_{33} = E_1\left(\tfrac{1}{a^2} + \beta^2 a^2\alpha_m^4 + 2\beta^2\alpha_m^2 n^2 + \tfrac{\beta^2}{a^2}n^4\right) + \tfrac{k_{A_r}}{a^2} + \left(k_{I_s} + \bar{z}_s^2 k_{A_s}\right)\alpha_m^4 + \tfrac{k_{J_r}+k_{J_s}}{a^2}\alpha_m^2 n^2$$
$$+ \tfrac{1}{a^2}\left(k_{I_r} + \tfrac{\bar{z}_r^2 k_{A_r}}{a^2}\right)n^4 + \tfrac{2}{a^3}\bar{z}_r k_{A_r} n^2 - \rho_t h\omega^2 + \rho_e\omega^2\tfrac{\mathrm{H}_n(\gamma a)}{\gamma\mathrm{H}_n'(\gamma a)} \tag{10}$$

The additional parameters are $\gamma = (k_e^2 - \alpha_m^2)^{\frac{1}{2}}$ with positive imaginary part, where $k_e = \omega/c_e$ is the acoustic wavenumber of the exterior fluid whose density is ρ_e and speed of sound is c_e, and whose loading on the shell is given by the term with H_n and H_n', the Hankel function of the first kind and its derivative with respect to its argument. This Hankel function is defined as $\mathrm{H}_n(z) = \mathrm{J}_n(z) + \mathrm{i}\mathrm{Y}_n(z)$, where $\mathrm{J}_n(z)$ and $\mathrm{Y}_n(z)$ are Bessel functions of the first and second kinds and z represents a general argument here rather than the coordinate axis. The recurrence relations for Bessel functions and Hankel functions – see Watson (1966) for instance – can be used to determine the derivative in terms of Hankel functions of order n and $(n+1)$, i.e. $\mathrm{H}_n'(z) = \frac{n}{z}\mathrm{H}_n(z) - \mathrm{H}_{n+1}(z)$. The same relation holds for the Bessel functions.

2.3 Excitation of the cylindrical shell due to an internal acoustic source

The rest of the solution follows that given in James (1985). A summary of that work is given in Pan, MacGillivray, Tso & Peters (2013) and the techniques are described in Skelton & James (1997). For an interior acoustic source, the excitation traction per unit area acting on the shell is given by the internal pressure p_i at the shell radius, that is

$$F_3(\phi, z) = p_i(a, \phi, z) \tag{11}$$

In the absence of any other types of loads on the shell, the axial and tangential tractions are $F_1 = F_2 = 0$, since the internal pressure can only couple to a surface in the normal direction, i.e. the radial direction for a shell with cylindrical geometry.

The internal pressure due to a monopole source is determined in James (1985) by taking the Green's function for a monopole between two rigid planes from Skelton (1985) and adding a modifying term for the scattering due to a rigid cylindrical enclosure corresponding to the dimensions of the cylindrical shell. The internal pressure p_i can be written as a series solution with terms like $\cos[q\pi(z+L)/2L]\,.\,cosn\phi.\,f_n(\gamma_q r)$, where f_n represents a Bessel function J_n or Y_n. Here it is assumed that the loading on the flexible shell will be the same as the pressure distribution over the inside of the acoustically rigid cylindrical enclosure. Taking the boundary condition at the cylindrical surface into account, the internal pressure loading on the shell can be written as a series which varies with axial mode number m, circumferential mode number n and the acoustic axial mode number q. However, in full form the terms in the series do not correspond to those in the series for the radial displacement. By ignoring the light fluid loading of the internal air and hence the coupling between shell structural modes via the air, the pressure series can be simplified and the modal loading terms on the shell are found to be

$$F_{3_{mn}} = \sum_{q=0}^{\infty} \frac{p_0 \epsilon_n \epsilon_q}{L\gamma_q a} \cos\frac{q\pi(z_0+L)}{2L} \frac{2m(1-(-1)^{m+q})}{\pi(m^2-q^2)} \frac{\mathrm{J}_n(\gamma_q r_0)}{\mathrm{J}'_n(\gamma_q r_0)} \tag{12}$$

where p_0 is the free-field amplitude of the point source, i.e. the monopole pressure at 1 m, located at $(r_0, 0, z_0)$, $\epsilon_n = 1$ for $n = 0$ and $\epsilon_n = 2$ for $n \geq 1$ and similarly for ϵ_q, and $\gamma_q = \left(k_i^2 - q^2\pi^2/4L^2\right)^{1/2}$ with positive real part where $k_i = \omega/c_i$ is the acoustic wavenumber in the internal fluid which has speed of sound c_i. Noting the assumed source position, this expression holds for all cases where the source circumferential angle is $\phi_0 = 0$. Notwithstanding this assumption, cylindrical symmetry can be used to calculate results with sources in other angular positions by applying the relative angular displacement to the coordinates of the observation point in the external fluid instead.

The force components defined by (12) vanish for all values of $(m+q)$ that are even including the case where $m = q$. Numerically, the former case can be handled easily as it just means a zero term added to the total sum. However, the latter case causes a numerical singularity using the expression for $F_{3_{mn}}$ above, so the $m = q$ condition must be tested for and the value of $F_{3_{mn}}$ explicitly set to zero when it is true. There are some special cases where simplifications can be applied. An example is when the acoustic source is exactly halfway along the cylinder, i.e. $z_0 = 0$, when only modes with odd m can be excited and consequently only even values of q need to be used with odd values of m to calculate a complete solution.

2.4 Far-field radiated pressure from the cylindrical shell

Lastly, the far-field radiated pressure p_{ef} is determined from the radial modal displacements W_{mn} of the cylindrical shell, which have been calculated from Equation (9) with the force components of Equation (12). The sound radiated from the finite-length cylinder is approximated by using the result for a cylinder with rigid semi-infinite cylindrical baffles extending from either end (indicated by fine dotted lines in Figure 1). The merits of this approximation are discussed in Junger & Feit (1993). Only the cylindrical surface contributes to the radiated sound. The expression for the far-field sound pressure is

$$p_{ef}(R, \theta, \phi) = -\frac{\mathrm{i}\omega\rho_e c_e \mathrm{e}^{\mathrm{i}k_e R}}{\pi R} \sum_{m=1}^{\infty} \sum_{n=0}^{\infty} \frac{G_{mn}(k_e \cos\theta)}{\sin\theta \mathrm{H}'_n(k_e a \sin\theta)} \mathrm{e}^{-\frac{\mathrm{i}n\pi}{2}} \cos n\phi \tag{13}$$

where the function G_{mn} contains the radial displacements W_{mn} and is defined as

$$G_{mn}(\alpha) = LW_{mn}\mathrm{e}^{\mathrm{i}\alpha L}.\frac{m\pi\left[1-(-1)^m \mathrm{e}^{-2\mathrm{i}\alpha L}\right]}{2L^2\ \left[m^2\pi^2/4L^2 - \alpha^2\right]} \tag{14}$$

The total displacements or pressures in the preceding equations are written as infinite sums over m, n and q. In

practice, a finite number of terms is sufficient to reach convergence for a given frequency range.

3. RESULTS & DISCUSSION

3.1 Shell and stiffener properties

The parameter values that were used to calculate results for this paper are given in Table 1. The shell and fluid parameters match those used to generate the numerical results given in James (1985). The shell and stiffeners are taken to be made of the same material, steel. While parameters are given for both ribs and stringers, these will be considered as two separate cases, a shell with ribs and a shell with stiffeners. The stiffeners are assumed to be T-beams of the same section for both ribs and stringers, with the base of the T attached to the inside of the shell. The beam section is characterised by the width of the flange b_f, the overall height of web plus flange d_o, and the thicknesses of the flange t_f and the web t_w. Figure 2 illustrates these dimensions. The stiffener spacing values are based on 15 ribs dividing the cylinder length into 16 bays, or 36 stringers spaced around the circumference.

Table 1: Material properties and geometry for the stiffened shell model

Parameter	Value
Length, $2L$ (m)	2.0
Radius, a (m)	1.0
Thickness, h (m)	0.010
Stiffener flange width, b_f (m)	0.060
Stiffener overall height, d_o (m)	0.070
Stiffener flange thickness, t_f (m)	0.006
Stiffener web thickness, t_w (m)	0.006
Spacing of 15 ribs, b (m)	0.125
Spacing of 36 stringers, d (m)	0.175
Young's modulus, E (GPa)	195
Shear modulus, G (GPa)	75.6
Poisson's ratio, v	0.29
Density, ρ (kg/m^3)	7700
Structural loss factor, η	0.02
Density of internal air, ρ_i (kg/m^3)	1.21
Speed of sound for air, c_i (m/s)	343
Loss factor for air, η_i	0.001
Density of external water, ρ_e (kg/m^3)	1000
Speed of sound for water, c_e (m/s)	1500

Formulae for the area properties of standard section shapes are available from a number of sources, such as Young & Budynas (2002). For the T-beam section, the area properties of the stiffeners that are required for either ribs or stringers are given by

$$A = b_f t_f + t_w(d_o - t_f)$$

$$y_c = \frac{1}{A}\left(\left(d_o - \frac{t_f}{2}\right) t_f b_f + \left(d_o - t_f\right)^2 \frac{t_w}{2}\right); \quad \bar{z} = y_c + \frac{h}{2}$$

$$I = t_w\left(d_o - t_f\right)\left(y_c - \frac{d_o - t_f}{2}\right)^2 + \frac{t_w\left(d_o - t_f\right)^3}{12} + t_f b_f \left(d_o - \frac{tf}{2} - y_c\right)^2 + \frac{t_f^3 b_f}{12}$$

$$J = \frac{1}{3}\left(b_f t_f^3 + t_w^3\left(d_o - \frac{t_f}{2}\right)\right) \tag{15}$$

which can be calculated from the overall dimensions given in Table 1. As indicated in Figure 2, the second moment of area I is that about the centroidal axis parallel to the top of the T; the centroidal distance $\bar{z}$ is the height of the centroid from the base of the T-section plus half the shell thickness. Since the ribs and stringers will be inside the shell, the negative value of this magnitude is used in the shell response calculations.

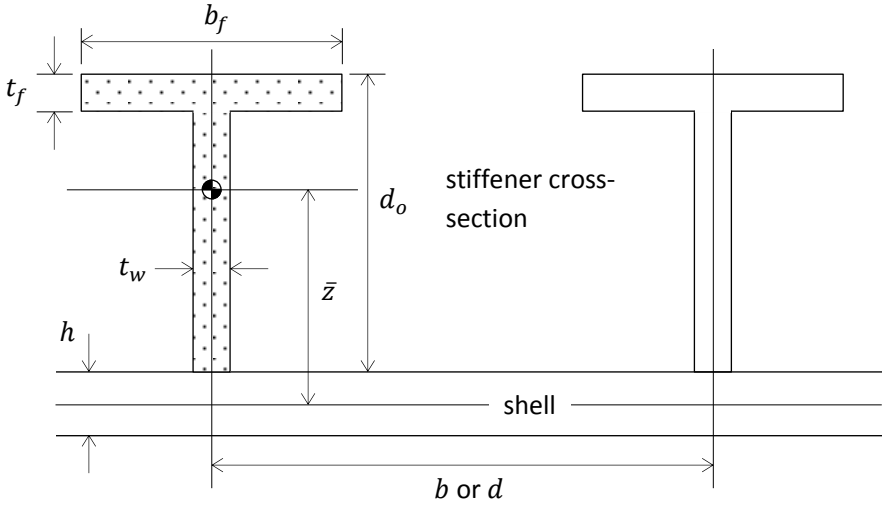

Figure 2: Dimensions for T-beam stiffeners in relation to the cylindrical shell. Cross-sectional area A is the shaded area, second moment of area I is about the horizontal axis through the centroid, and torsion constant J is about the axis through the centroid out of the plane of the page.

3.2 Other computational parameters

The equations for the cylinder response, internal pressure excitation and far-field radiated pressure were coded in MATLAB. The results for far-field radiated pressure at $R = 1000$ m, $\theta = 90°$ and $\phi = 0$ were calculated for a single monopole source of strength $p_0 = 1$ Pa placed inside the cylinder at $r_0 = 2a/3 = 0.67$ m, $\phi_0 = 0$ and $z_0 = L/10 = 0.1$ m. This source strength corresponds to a sound pressure level of 94 dB re 20 µPa (or 120 dB re 1 µPa). The far-field radiated sound pressure level is normalised back to 1 m by adding 60 dB, based on a spherical spreading assumption for the sound radiating into the water.

The frequency range considered was up to 500 Hz. The number of terms used in the summations were m values up to 15, n values up to 10 and q values up to 20. These values gave convergence to the original results in James (1985) for axially central acoustic excitation, although they are probably higher than needed. Nevertheless, the results calculated in MATLAB in less than 10 seconds on a relatively recent (2014 model) quad-core laptop computer.

A note on acoustic damping is in order. The effect of a layer of fibreglass sound absorbing material on the internal cylinder wall was incorporated in the modelling presented in Pan, Tso, Forrest & Peters (2014). The damping effect of this is quite high, significantly reducing the levels of the peaks in the calculated far-field radiated pressure, which is dominated by the radiation of internal acoustic modes of the cylinder. While this has useful practical implications, it also somewhat obscures the behaviour of the radiating cylinder. Since the purpose of the present paper is to examine the effect of structural stiffeners, only a light value of damping using a loss factor of

$\eta_i = 0.001$ for the internal air, as indicated in Table 1, is used to tame the peak excursions of the radiated pressure.

3.3 Calculated results

The results for the shell with added ribs are plotted in Figure 3 and those for the shell with added stringers are plotted in Figure 4. In each case, the far-field radiated pressure is given for the plain isotropic shell without any stiffeners, the shell with only the equivalent mass of the stiffeners added through the effective density ρ_t, and the shell with the complete smeared-stiffener description given by the spectral response coefficients (10) used in the matrix equation (9). Other rib or stringer parameters are set to zero as necessary for each response calculated. Note that levels are higher than the 120 dB re 1 µPa free-field source level, due to the build-up of a reverberant sound field inside the cylinder. This can be understood qualitatively as follows. Sound intensity magnitude I for a plane wave is $I =< p^2 >/\rho c$ (Bies & Hansen, 1996). Since pressures must be equal $p_i = p_e$ at the cylindrical boundary, but the water has a much higher impedance $\rho_e c_e$ than $\rho_i c_i$ for the air, the amount of energy I transferred out per unit surface area is a small proportion of the total incident energy and most is reflected back into the enclosure, adding to the reverberant field.

James (1985) notes that the sharp peaks observed for the plain cylindrical shell of this size correspond to internal acoustic modes radiating. A number of efficiently radiating shell structural modes also show up in the black curve in Figure 3 or Figure 4, but at lower levels than the peaks due to the internal acoustic modes. Partly this is a function of the higher structural damping ($\eta = 0.02$) compared to the low acoustic damping ($\eta_i = 0.001$). These include more subdued peaks at about 118 Hz, 203 Hz (just to the right and on the side of the highest peak), 262 Hz and 319 Hz. These occur at structural modes (m, n) noted by James (1985) as the (1, 2), (1, 1), (3, 4) and (3, 3) modes. Other structural modes in the range that do not show up in the radiated sound pressure include (1,3) at 79 Hz, (3,2) at 365 Hz and (3,1) at 406 Hz. The modes noted for the plain shell do not exceed $m = 3$ or $n = 4$ in the frequency range up to 500 Hz, for both structural and internal acoustic modes. This indicates both that the summation ranges chosen were sufficient, and that the assumption of structural wavelengths being greater than the stiffener spacings is satisfied for the parameters used. There is scope to explore this further by automatically selecting the number of terms needed for the solution of a particular case based on the structural and acoustic natural frequencies of the cylindrical enclosure. The structural part could be dealt with by solving for ω^2 as the natural frequency squared in the characteristic equation that arises from setting the determinant of the matrix in Equation (9) to zero, i.e. solving for the non-trivial solutions when the forces are zero, over a range of (m, n) values.

Adding rib mass, the blue curve in Figure 3, has little effect on the peaks due to acoustic modes below about 250 Hz, but does lower the frequencies of the peaks due to structural modes. The effect of added mass only is more mixed above 250 Hz. The use of the full smeared rib stiffener terms, the red curve, leads to reductions in peak levels for all the peaks at 271 Hz and below. The contributions of the structural modes in this range either disappear or are much diminished. Presumably these effects are due to the much greater radial stiffness that circumferential ribs provide and hence lower levels of radial displacement induced by the internal acoustic pressure. At the higher frequencies up to 500 Hz the picture is more complicated, with notable increases in peak level at 291 Hz and 466 Hz while many other peaks are reduced or similar in level compared to previously. The added ribs appear to have resulted in a significant improvement in sound transmission at these two high peaks.

Adding stringer mass, the blue curve in Figure 4, also has little effect on the peaks due to acoustic modes, but across most of the frequency range this time. The peaks due to structural modes are again lowered in frequency. The use of full smeared stringer terms, the red curve, also appears to have little effect below about 300 Hz. Here, most of the structural modal terms have $m = 1$ and these are what contribute to the shell response, even off-resonance to acoustic modal peaks in the excitation pressure due to the internal noise source. Bending the stringers into a half-wavelength only does not add much apparent stiffness to the shell response and the far-field radiated pressure remains similar to the other curves. Above 300 Hz, much of the radiated pressure curve is reduced compared to previously. Here, higher values of m contribute to the shell response, and since the stringers then experience more cycles of bending along their length in these contributing modal terms, the increase in apparent stiffness is greater and the shell response is reduced.

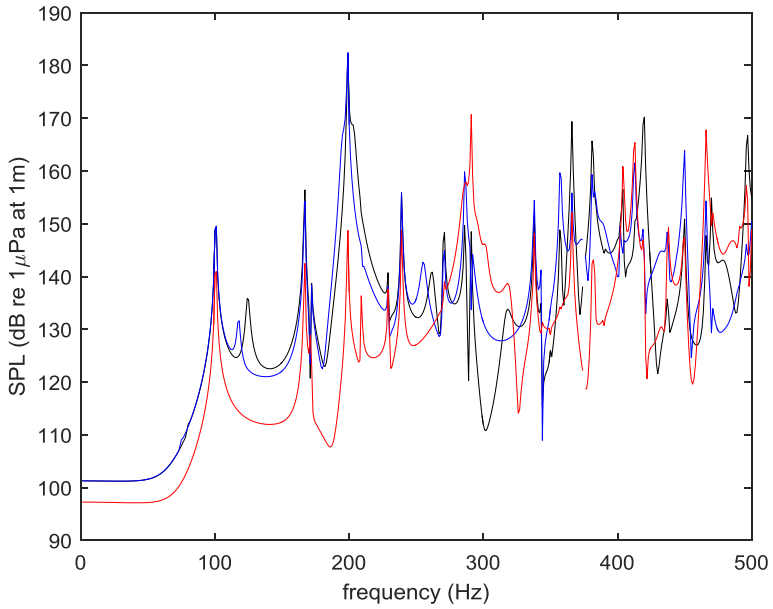

Figure 3: Far-field radiated pressure for plain shell —, with added rib mass —, with full rib terms —

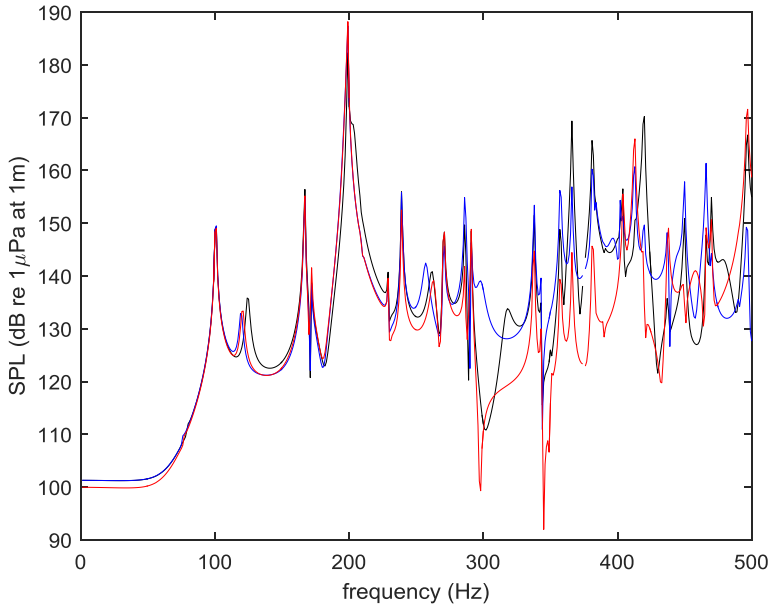

Figure 4: Far-field radiated pressure for plain shell —, with added stringer mass —, with full stringer terms —

4. CONCLUSIONS

An analytical model for the sound radiated from an underwater cylindrical enclosure with an internal noise source has been demonstrated. The model includes allowance for ribs and/or stringers by representing them as extra smeared mass and stiffness parameters added to the cylindrical shell representing the enclosure. The scattered sound field due to a monopole source in the cylindrical volume provides the internal pressure loading on the cylinder walls; the response of the cylinder is calculated using this loading as the forcing term in a thin-shell theory formulation including external fluid loading; and the far-field radiated sound is then calculated using the cylindrical shell response as the input to an expression for this.

The model can be used to calculate typical results very quickly on a laptop computer. The results for far-field radiated pressure up to 500 Hz given in this paper for a 2 m diameter steel shell of 2 m length show peaks that are due to a mixture of internal acoustic modes (giving high shell excitation at their resonances) and efficiently radiating structural modes. The addition of stiffener mass alone changes the peaks due to the acoustic modes very little and shifts the peaks due to structural modes down in frequency. The inclusion of a full representation of rib stiffeners reduces all the peak responses for the lower part of the frequency range, while having a mixed effect on peak responses in the upper part of the frequency range. The peaks due to the structural modes either disappear or are much reduced. This indicates that the rib stiffeners generally have a large effect on radial stiffness, reducing the radial response of the shell and thus the radiated sound pressure. The inclusion of a full representation of stringer stiffeners has little effect on the peaks due to acoustic modes in the lower part of the frequency range, with only some shift in frequency of peaks due to structural modes. Many of the peaks in the upper part of the frequency range, however, are reduced quite significantly. This seems to be because the axial structural wavenumber is larger in the upper frequency range, so the bending stiffness of the longitudinal stringers has more effect on overall radial stiffness of the shell than in the lower frequency range.

Future work could include exploring the automatic selection of the number of terms needed for the solution of a particular case based on the structural and acoustic natural frequencies of the cylindrical enclosure. This could be approached by solving for the cylindrical shell structural natural frequencies over a range of (m, n) values and for the cylindrical acoustic volume natural frequencies over a range of (m, n, q) values. The number of terms required would be informed by the highest mode numbers obtained from all the natural frequencies that fall within the frequency range of interest.

ACKNOWLEDGEMENTS

The author would like to thank Xia Pan and Paul Dylejko, whose MATLAB code for a uniform shell was used as the starting point for the generation of the results presented in this paper.

REFERENCES

Bies, DA & Hansen, CH 1996, *Engineering Noise Control – Theory and Practice*, 2nd edition, Spon Press, London.

Forrest, JA 2011, 'Structural vibration transmission in stiffened structures', *Proceedings of Acoustics 2011*, 2-4 November 2011, Gold Coast, Australia.

Forrest, JA 2014, 'Modelling the forced response of a stiffened structure', *Proceedings of Inter-Noise 2014*, 16-19 November 2014, Melbourne, Australia.

James, JH 1985, 'An approximation to sound radiation from a simply-supported cylindrical shell excited by an interior point source', AMTE(N) TM85024, Admiralty Marine Technology Establishment, Teddington, UK.

Junger, MC & Feit, D 1993, *Sound, Structures and Their Interaction*, Acoustical Society of America, New York.

Leissa, A 1993, *Vibration of Shells*, Acoustical Society of America, New York.

Mikulas, MM & McElman, JA 1965, 'On free vibrations of eccentrically stiffened cylindrical shells and flat plates', NASA TN D-3010, National Aeronautics and Space Administration, Washington D.C.

Pan, X, MacGillivray, I, Tso, Y & Peters, H 2013, 'Investigation of sound radiation from a water-loaded cylindrical enclosure due to airborne noise', *Proceedings of Acoustics 2013*, 17-20 November 2013, Victor Harbor, Australia.

Pan, X, Tso, Y, Forrest, J & Peters, H 2014, 'Sound radiation from a water-loaded cylinder due to machine noise', *Proceedings of Inter-Noise 2014*, 16-19 November 2014, Melbourne, Australia.

Skelton, EA 1985, 'Green's function of the reduced wave equation between parallel planes', AMTE(N) TM85025, Admiralty Marine Technology Establishment, Teddington, UK.

Skelton, EA & James, JH 1997, *Theoretical Acoustics of Underwater Structures*, Imperial College Press, London.

Watson, GN 1966, *A Treatise on the Theory of Bessel Functions*, 2nd edition, Cambridge University Press, London.

Young, WC & Budynas, RG 2002, *Roark's Formulas for Stress and Strain*, 7th edition, McGraw-Hill, New York.